Supplemental Material for "Possible chiral spin liquid state in the $S = 1/2$ kagome Heisenberg model"

Rong-Yang Sun[1,2,3,*], Hui-Ke Jin[4,*], Hong-Hao T[5,†], Yi Zhou[6,7,3,8,‡]

[1]Computational Materials Science Research Team,
RIKEN Center for Computational Science (R-CCS), Kobe, Hyogo, 650-0047, Japan
[2]Quantum Computational Science Research Team,
RIKEN Center for Quantum Computing (RQC), Wako, Saitama, 351-0198, Japan
[3]Kavli Institute for Theoretical Sciences,
University of Chinese Academy of Sciences, Beijing 100190, China
[4]Department of Physics TQM, Technische Universität München,
James-Franck-Straße 1, D-85748 Garching, Germany
[5]Institut für Theoretische Physik, Technische Universität Dresden, 01062 Dresden, Germany
[6]Institute of Physics, Chinese Academy of Sciences, Beijing 100190, China
[7]Songshan Lake Materials Laboratory, Dongguan, Guangdong 523808, China
[8]CAS Center for Excellence in Topological Quantum Computation,
University of Chinese Academy of Sciences, Beijing 100190, China
[*]These two authors contributed equally
email: [‡]hong-hao.tu@tu-dresden.de, [†]yizhou@iphy.ac.cn

September 8, 2022

This Supplemental Material includes more numerical details about energetic comparison between Random-DMRG and Boosted-DMRG, chirality estimation in the CSL phase, finite-size gaps between two topological sectors, and edge spinons in the semion sector.

Supplementary Note 1: Ground-state energy comparisons and re-diagonalization

We first introduce the relative energy difference between two close energies, E_1 and E_2, as

$$\delta(E_1, E_2) \equiv \left| \frac{E_1 - E_2}{(E_1 + E_2)/2} \right| . \tag{1}$$

Supplementary Table 1: Relative energy difference between Random-DMRG and Boosted-DMRG states, $\delta(E_{\mathrm{RD}}, E_{\mathrm{BD}})$, and between two re-orthogonalized states, $\delta(\tilde{E}_1, \tilde{E}_2)$, in the CSL phase on a 224-site YC8 cylinder.

J'	$\delta(E_{\mathrm{RD}}, E_{\mathrm{BD}})$	$\delta(\tilde{E}_1, \tilde{E}_2)$
0.08	1.81×10^{-9}	3.13×10^{-7}
0.07	1.92×10^{-7}	2.39×10^{-6}
0.06	1.50×10^{-7}	2.44×10^{-6}
0.05	9.96×10^{-8}	1.92×10^{-6}
0.04	1.35×10^{-7}	4.73×10^{-6}
0.03	9.97×10^{-9}	2.82×10^{-5}
0.02	1.72×10^{-7}	4.11×10^{-6}
0.01	1.29×10^{-7}	3.44×10^{-6}
0	6.45×10^{-8}	1.13×10^{-5}
-0.01	4.42×10^{-7}	9.79×10^{-7}
-0.02	1.61×10^{-6}	2.63×10^{-6}
-0.03	1.49×10^{-6}	4.90×10^{-6}

As mentioned in the main text, we obtained two almost degenerate ground states, $|\Psi_{\mathrm{RD}}\rangle$ and $|\Psi_{\mathrm{BD}}\rangle$, by using Random-DMRG and Boosted-DMRG, respectively. In the CSL phase, these two states are generally not orthogonal to each other. Denoting the variational energy of $|\Psi_{\mathrm{RD}}\rangle$ ($|\Psi_{\mathrm{BD}}\rangle$) as E_{RD} (E_{BD}), the relative energy difference $\delta(E_{\mathrm{RD}}, E_{\mathrm{BD}})$ is extremely small, as listed in Table 1.

With two non-orthogonal MPSs $|\Psi_{\mathrm{RD}}\rangle$ and $|\Psi_{\mathrm{BD}}\rangle$ in hand, we carry out a further variational optimization to obtain re-orthogonalized states and corresponding energies. This optimization is formulated as a generalized eigenvalue problem by contructing the following 2×2 matrices:

$$H_2 = \begin{pmatrix} \langle \Psi_{\mathrm{RD}} | H | \Psi_{\mathrm{RD}} \rangle & \langle \Psi_{\mathrm{RD}} | H | \Psi_{\mathrm{BD}} \rangle \\ \langle \Psi_{\mathrm{BD}} | H | \Psi_{\mathrm{RD}} \rangle & \langle \Psi_{\mathrm{BD}} | H | \Psi_{\mathrm{BD}} \rangle \end{pmatrix}, \tag{2}$$

and

$$N_2 = \begin{pmatrix} \langle \Psi_{\mathrm{RD}} | \Psi_{\mathrm{RD}} \rangle & \langle \Psi_{\mathrm{RD}} | \Psi_{\mathrm{BD}} \rangle \\ \langle \Psi_{\mathrm{BD}} | \Psi_{\mathrm{RD}} \rangle & \langle \Psi_{\mathrm{BD}} | \Psi_{\mathrm{BD}} \rangle \end{pmatrix}. \tag{3}$$

By solving the generalized eigenvalue problem, namely, $H_2 x = E N_2 x$, we can obtain two re-diagonalized eigen-energies, $\tilde{E}_1$ and $\tilde{E}_2$. The relative energy difference $\delta(\tilde{E}_1, \tilde{E}_2)$, with respect to newly obtained $\tilde{E}_1$ and $\tilde{E}_2$, is listed in Table 1.

Supplementary Note 2: Spin chirality

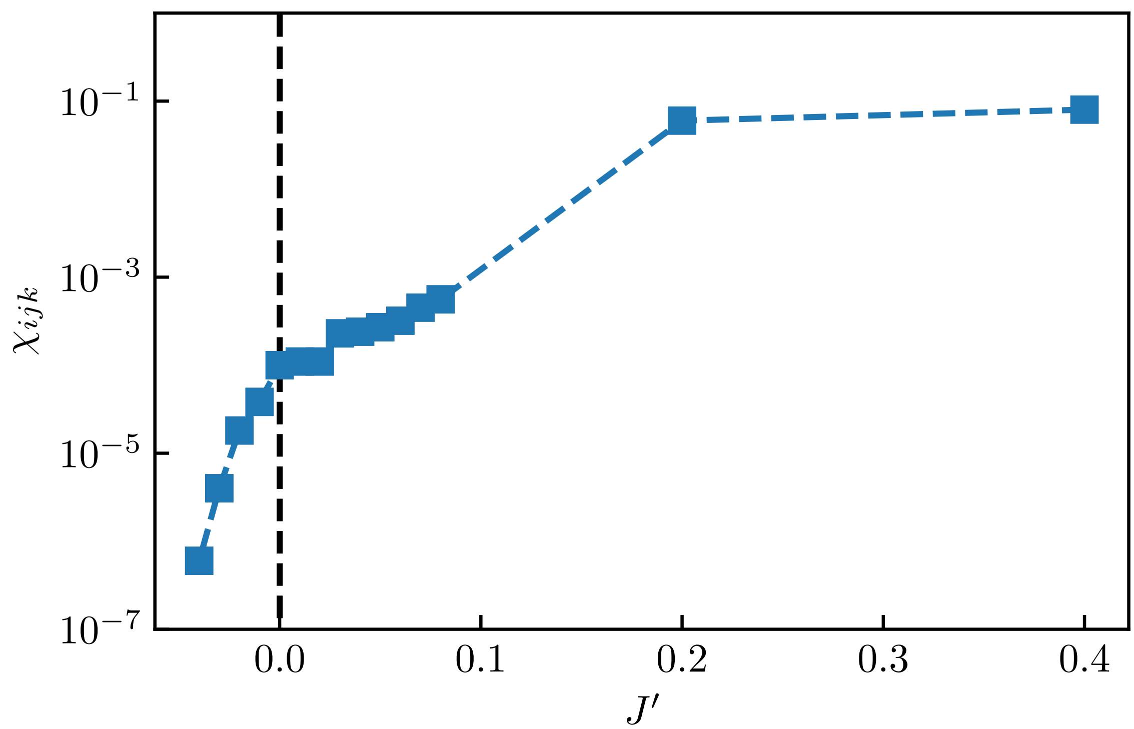

Supplementary Figure 1: χ_{ijk} on an elementary triangle in the center of a 224-site YC8 cylinder as a function of J'.

In order to characterize the chirality, we define the three-spin operator on an elementary triangle $\triangle_{ijk}$ [see the elementary triangles in Fig. 1(b)] as

$$E_{ijk} = \mathbf{S}_i \cdot (\mathbf{S}_j \times \mathbf{S}_k)\,. \tag{4}$$

Notice that E_{ijk} is purely imaginary and Hermitian, indicating that $\langle\psi|E_{ijk}|\psi\rangle = 0$ for any real state $|\psi\rangle$.

In the CSL phase, we can obtain two orthogonal degenerate ground states, $|\tilde{\Phi}_1\rangle$ and $|\tilde{\Phi}_2\rangle$, by the re-diagonalization method introduced above. Because both $|\tilde{\Phi}_1\rangle$ and $|\tilde{\Phi}_2\rangle$ are real wave functions, the expectation values of E_{ijk} with respect to those two states must be zero. Nevertheless, we can evaluate the spin chirality by introducing the following 2×2 matrix:

$$\chi_2(ijk) = \left(\begin{array}{cc} 0 & \langle\tilde{\Phi}_1|E_{ijk}|\tilde{\Phi}_2\rangle \\ \langle\tilde{\Phi}_2|E_{ijk}|\tilde{\Phi}_1\rangle & 0 \end{array} \right). \tag{5}$$

It is easy to verify that $\chi_2(ijk)$ is Hermitian and has symmetric eigenvalues with respect to zero, namely, $\pm\chi_{ijk}$ ($\chi_{ijk} > 0$), corresponding to chiral and anti-chiral ground states, respectively. Hereafter we choose the elementary triangle $\triangle_{ijk}$ in the center of a YC8 cylinder to compute χ_{ijk}. Notice that there are two types of elementary triangles corresponding to up- and down-triangles and they give rise to almost the same results. For relatively large J' ($J' = 0.2$), we find that $\chi_{ijk} \approx 0.06$ which is very close to the result obtained in Ref. [**?**]. As shown in Supplementary Fig. 1, χ_{ijk} decreases as J' decreases. At the point of $J' = 0$, we find that $\chi_{ijk} \approx 1.0 \times 10^{-4}$, and at the transition point between the VBC II and CSL phases ($J' = -0.04$), $\chi_{ijk} \approx 6.0 \times 10^{-7}$ is almost zero.

Supplementary Note 3: Finite-size gap between identity and semion sectors

Although the ground states in the identity and semion sectors, namely, $|\Psi_{\mathrm{I}}\rangle$ and $|\Psi_{\mathrm{S}}\rangle$, are degenerate in the thermodynamic limit, a finite energy gap between these two states always exists

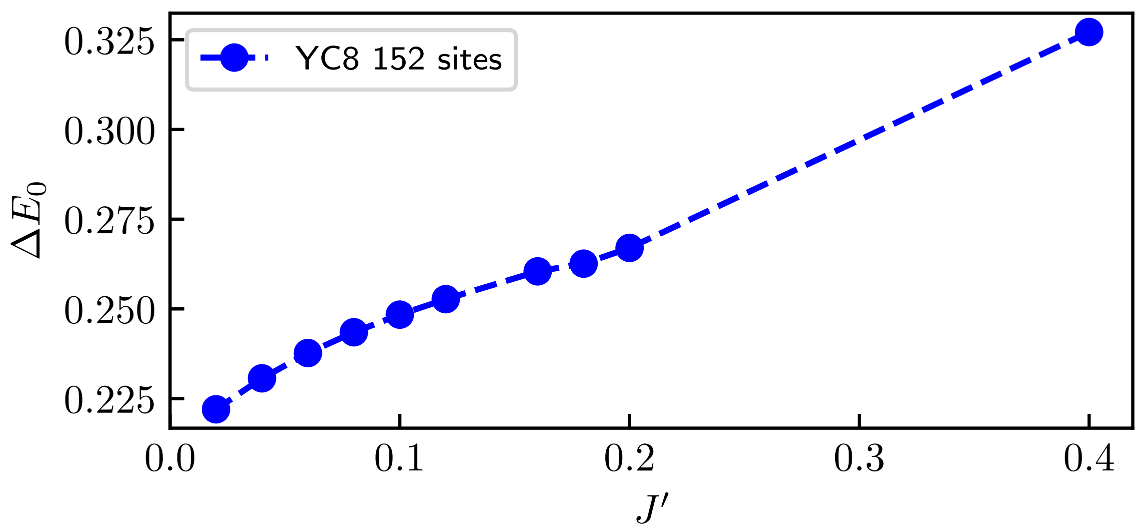

Supplementary Figure 2: The finite energy gaps between $|\Psi_{\mathrm{I}}\rangle$ and $|\Psi_{\mathrm{S}}\rangle$ on a 152-site YC8 cylinder.

in finite-size systems. In Supplementary Fig. 2, we show that this finite-size gap decreases with J' in the regime of $0.02 \le J' \le 0.4$.

Supplementary Note 4: Localization length of the edge semions

For the ground state in the semion sector, we measure the total magnetization on the i-th column, M_i^z, as

$$M_i^z = \sum_j \langle \Psi_{\mathrm{S}} | S_{i,j}^z | \Psi_{\mathrm{S}} \rangle, \tag{6}$$

where i and j are column and row indices, respectively, and the summation $\sum_j$ runs over all the lattice sites belonging to the i-th column. In Supplementary Fig. 3, we show the M_i^z profile for various J'. Clearly, the localization lengths of two semions at the boundaries of the cylinder increase as J' decreases, from which it is expected that the localization length of each edge semion might be as large as half of the cylinder length when J' is close to $J' = 0$.

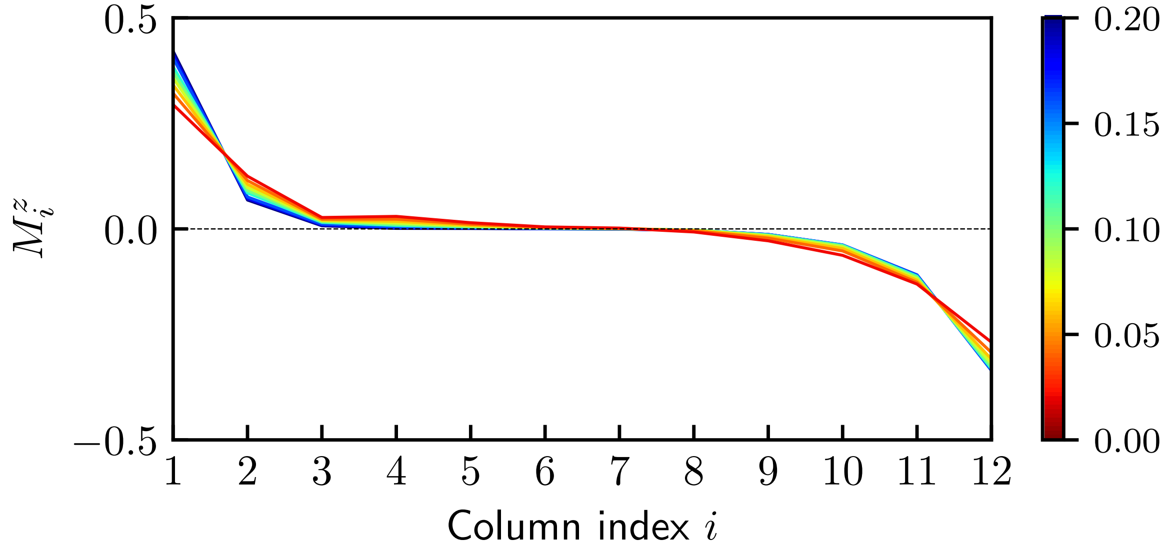

Supplementary Figure 3: The evolution of the column summation of the M_i^z distribution of semion sector states in the 152-site YC8 system from $J' = 0.2$ to $J' = 0.02$. The coupling J' for each curve can be read from the colorbar.